Size comparison of Closed sCO_2 Brayton Cycle and Open Air Brayton Cycle for Molten Salt Reactor applications

Taeyeon Min [a], Jeong Ik Lee [a*]
[a]*Department of Nuclear and Quantum Engineering, Korea Advanced Institute of Science and Technology; 373-1 Guseong-dong Yuseong-gu, Daejeon 305-701, Republic of Korea*
[*] *Correspinding author: jeongiklee@kaist.ac.kr*

Keywords : Molten Salt Reactor, Plate Fin type Heat Exchanger, Printed Circuit Heat Exchanger

1. Introduction

In a small reactor, the size of the entire system is an important factor. The smaller the size of the system, the more directly linked to the higher the installation autonomy and the reduction of the installation cost. The molten salt reactor (MSR) consists of a primary loop that transfers the heat of the core, an intermediate loop that transfers the heat stably, and a power conversion cycle. [1] Since the power conversion cycle of MSR operates at high temperatures, the Gas Brayton Cycle with high thermal efficiency is used. Typically adopted cycles include the Open-Air Brayton Cycle (OABC) and the Closed supercritical CO_2 Brayton Cycle (CCBC) [2]. Meanwhile, a compact heat exchanger has been developed because the size of the heat exchanger in the power conversion system is related to economic feasibility. Compact heat exchangers include printed circuit heat exchanger (PCHE), plate fin heat exchanger (PFHE), and micro shell and tube heat exchanger (MSTE) [3]. In 2022, Son et al suggested PFHE for heat exchanger of OABC and evaluated optimal pinch temperature of MSR of heat exchanger system [4]. In this study, a comparative analysis focusing on size was conducted between the CCBC and the OABC, both of which are viable power conversion cycles for MSRs. To elucidate the distinctions between each power conversion cycle, a preliminary thermal sizing evaluation was executed.

2. Method and Results

2.1 Cycle Optimization and Thermal Sizing

In this study, primary loop design parameters are selected as shown in Table 1. Optimization of both Brayton cycle for core heat load of $6.5MW_{th}$ and maximum temperature of 650°C was performed. Pinch temperature is selected to 10K, which the difference between maximum temperature of connected each cycle.

Table 1. Design parameters of primary loop

	Value
Hot side inlet Temperature.	650°C
Heat Load	$6.5MW_{th}$
Pinch Temperature	10K

Figure 1 is the OABC layout and CCBC layout used in this study. For the Air cycle, air enters the compressor and exit through the recuperator. The air minimum temperature was selected to 15°C that represent the highest cycle thermal efficiency by Son (2022). In case of sCO_2 cycle, the precooler exists additionally, and maximum sCO_2 pressure was selected to 25MPa for the same reason of Air power cycle. Both design parameter is selected as shown Table 2 [5] [6]. In OABC, Conventionally, the HX pressure drop was determined in proportion to the system pressure using reasonable numbers used in the design. Cycle optimization was performed by using an in-house code of which name is KAIST-OCD and KAIST-CCD. A numerical method is used to find the optimal pressure ratio, which has the highest cycle efficiency. which has the highest cycle efficiency. The algorithm of this code is shown in Figures 2 and 3, respectively. Meanwhile, the results of optimization are shown in Table 3.

Table 2. Design parameters of the Open-Air Brayton Cycle and Closed sCO_2 Brayton Cycle

Open Air Brayton Cycle		**Closed sCO_2 Brayton Cycle**	
Air intake Temperature/Humidity	15°C/Dry	Max Pressure	25MPa
Max Temperature	630°C	Max Temperature	60°C
Compressor Inlet Pressure	101.325 kPa	Min Temperature	630°C
Turbine efficiency	90%	Turbine efficiency	90%
Compressor efficiency	86%	Compressor efficiency	86%
Recuperator effectiveness	92%	Recuperator effectiveness	92%
Generator Efficiency	96%	Thermal Heat	6.5 MW
Component ΔP ratio	-	Component pressure drop	100-250 kPa
HX Cold side ΔP ratio	0.03	Heater Cold side	150 kPa
Recuperator Hot side ΔP ratio	0.03	Recuperator Hot side	250 kPa
Recuperator Cold side ΔP ratio	0.03	Recuperator Cold side	100 kPa
Ratio of exhaust pressure to atmosphere	0.98	Cooler Hot side	100 kPa

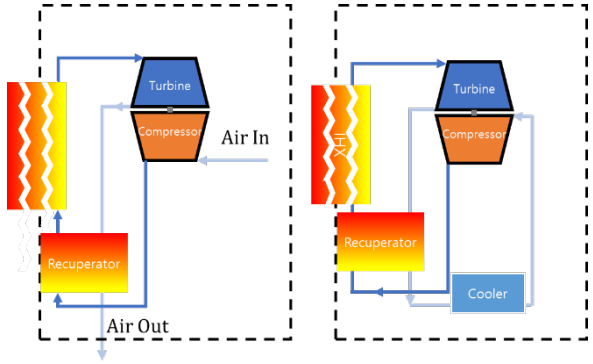

Figure 1. Air recuperated power Brayton open cycle and sCO2 recuperated power Brayton closed cycle

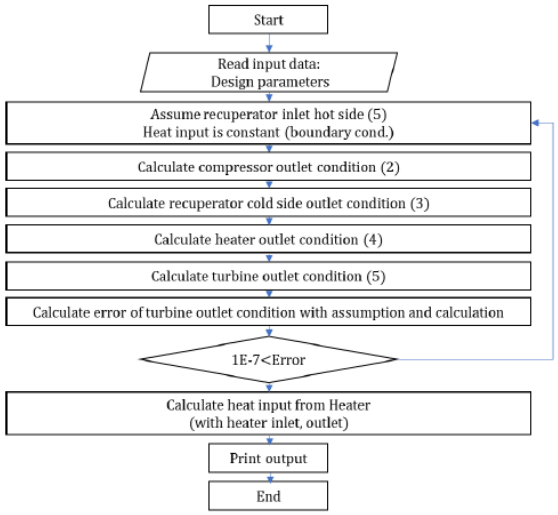

Figure 2. Algorithm of KAIST-OCD

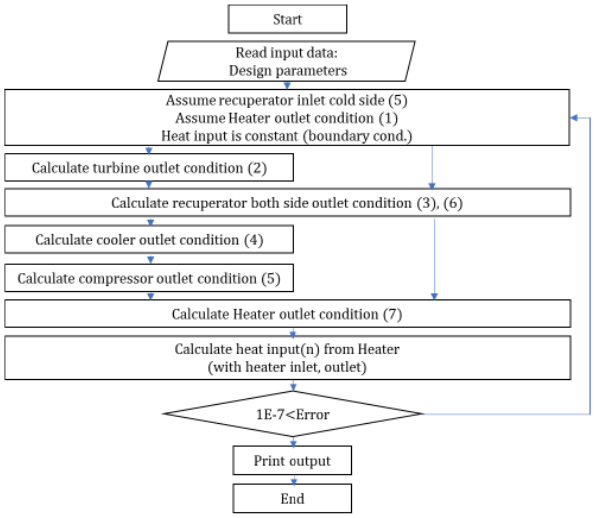

Figure 3. Algorithm of KAIST-CCD

Table 3. Optimization result of Power conversion cycle

	OABC	CCBC
Cycle Net Efficiency [%]	34.6	34.7
Pressure Ratio	2.49	2.83
Mass flow rate [kg/s]	29.9	25.5

To design the secondary heat exchanger, the thermal sizing of the secondary loop fluid was performed. The fluid is selected by FLiBe. Since the fluid should exhibit a stable liquid state in the intermediate loop, the minimum temperature was set at 590°C, which is above the melting point of FLiBe. Meanwhile, it is chemically stable at the temperature interval of application [7]. Thermal sizing parameters with thermal sizing results were assumed to Table 4, which include heat exchanger inlet and outlet fluid conditions of intermediate loop side by referring values from the previous works [8]. The used thermal properties and correlation are summarized in Table 5.

Table 4. Design parameters of secondary heat exchanger of OABC and CCBC

	OABC		CCBC	
	Intermediate loop	Power conversion loop	Intermediate loop	Power conversion loop
Inlet/outlet Temperature [°C]	640/590	432.3/630	640/590	426.7/630
Inlet Pressure [kPa]	531	274	150	24900
Pressure drop	300kPa	8.22kPa	50kPa	150kPa
Mass flow rate [kg/s]	54.5	29.9	54.5	25.5

Table 5. Thermal Properties of FLiBe

Specific heat $\left[\frac{J}{kg*K}\right]$	2.386×1000
Density $\left[\frac{kg}{m^3}\right]$	$(2.518 - 0.000406 \times (T - 273.15)) \times 1000$
Dynamic viscosity $\left[\frac{kg}{m*s}\right]$	$\left(0.0116 \times exp\left(\frac{3755}{T}\right)\right) \times 0.01$
Thermal conductivity $\left[\frac{W}{m*K}\right]$	$0.0005 \times (T - 273.15) + 0.6297$

2.2 Heat Exchanger Desing for Open Air Brayton Cycle

In this study, PFHEs are selected to exchange heat for Air Open Brayton cycles. PFHE is a heat exchanger that consists of alternating layers of corrugated fins and flat separators. The fin types for PFHE include plain, louver, and offset strip. Among them, offset strip fins have a high convective heat transfer coefficient because of low average boundary-thickness [9]. Therefore, offset strip fins type is selected in this study for design and analysis. The selected MSR heat exchanger is a counter-flow type and offset strip fins with a rectangular cross section is shown as Figure 4A, 4B. As shown in Figure 4B, fin consists of fin gap $(= s)$, fin height $(= h)$, fin - thickness $(= t)$, and fin offset length $(= l)$ for the

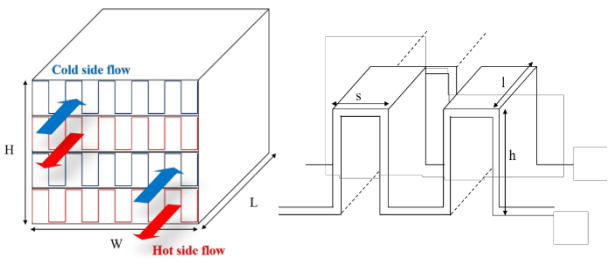

Figure 4. (A) schematic of counter-flow plate-fin heat exchanger, (B) Detailed view of the offset-strip fin

hot and cold sides of the heat exchanger. The PFHE is optimized through changing the fin gap, fin height, fin offset length, number of fin layers, and the width and length of the heat exchanger. To minimize heat loss in PFHE design, the number of cold fin layers is always set more than the number of hot fin layers by unity.

The correlation of the j and f factors for the offset strip fin shape are the following Equation 1 and 2, which is suggested by Manglik and Bergles [10].

$$j = 0.6522Re^{-0.5403}\left(\frac{s'}{h'}\right)^{-0.1541}\left(\frac{t}{l}\right)^{0.1499}\left(\frac{t}{s'}\right)^{-0.0678} \times\left[1+5.269\times10^{-5}Re^{1.340}\left(\frac{s'}{h'}\right)^{0.504}\left(\frac{t}{l}\right)^{0.456}\left(\frac{t}{s'}\right)^{-1.055}\right]^{0.1} \quad (1)$$

$$f = 9.6243Re^{-0.7422}\left(\frac{s'}{h'}\right)^{-0.1856}\left(\frac{t}{l}\right)^{0.3053}\left(\frac{t}{s'}\right)^{-0.2659} \times\left[1+7.669\times10^{-8}Re^{4.429}\left(\frac{s'}{h'}\right)^{0.902}\left(\frac{t}{l}\right)^{3.767}\left(\frac{t}{s'}\right)^{0.236}\right]^{0.1} \quad (2)$$

where $s' = s - t$, $h' = h - t$, Re is the Reynolds number defined as $Re = \frac{GD_h}{\mu}$. Hydraulic diameter defined as $D_h = \frac{4sh'l}{2(sl+h'l+th')+ls]}$, G is the mass flux which is defined $G = \frac{m}{A_{flow}}$. The Equation 1 and 2 is valid for $0.134 < \frac{s'}{h'} < 0.997, 0.012 < \frac{t}{l} < 0.048, 0.041 < \frac{t}{s'} < 0.0121$ [10].

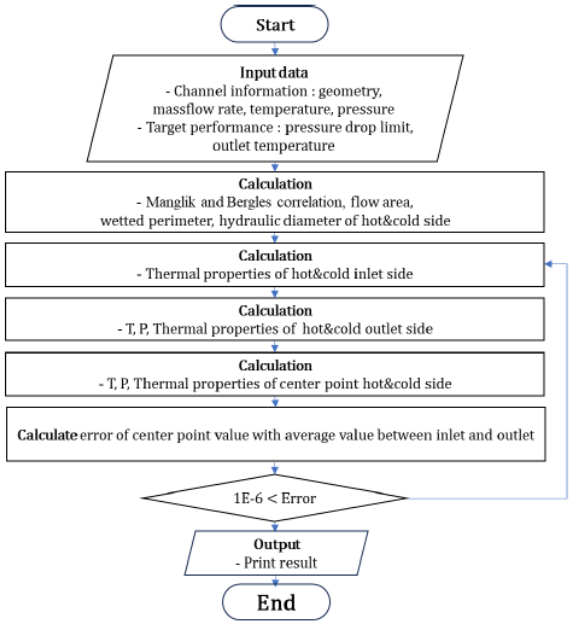

Figure 5. Algorithm of KAIST-PFHE

For the secondary heat exchanger design optimization, design parameters of secondary heat exchanger assumed in Table 6, which referred to the previous work [9]. The plate material is selected as SS316L, and thickness is set to 0.5 mm based on the previous studies [9]. In addition, design parameters of intermediate loop and power conversion loop are shown in Table 4 above. Likewise, for the recuperator design optimization, design parameters of the recuperator were assumed in Table 6. Meanwhile, the design parameters of hot and cold side of the recuperator are shown in Table 7, which is obtained from cycle optimization.

The optimization process was carried out using the in-house code which is called KAIST-PFHE. The algorithm of this code is shown in Figure 5. In the design of the heat exchanger that satisfies the following conditions, the size of the heat exchanger with the smallest volume was calculated, and the results are as follows. The results of both cases are shown in Table 8. The core volume of secondary heat exchanger and recuperator is the smallest by 0.724m^3 and 9.88m^3.

Table 6. Design parameters of PFHE

	Secondary Heat Exchanger		Recuperator	
	Hot	**Cold**	**Hot**	**Cold**
Minimum Fin Thickness	0.1×10^{-3}m	0.3×10^{-3}m	0.1×10^{-3}m	0.3×10^{-3}m
Gap Range	0.4×10^{-3}m ~1.4×10^{-3}m	2.8×10^{-3}m ~4.3×10^{-3}m	3.0×10^{-3}m ~4.8×10^{-3}m	4.0×10^{-3}m ~5.8×10^{-3}m
Height Range	0.2×10^{-3}m ~1.8×10^{-3}m	3.5×10^{-3}m ~5.3×10^{-3}m	1.8×10^{-3}m ~3.3×10^{-3}m	2.8×10^{-3}m ~4.3×10^{-3}m
Width Range	0.8m~2.0m		0.8m~2.0m	
Fin Length Range	3×10^{-3}m ~8×10^{-3}m	7×10^{-3}m ~25×10^{-3}m	3×10^{-3}m ~8×10^{-3}m	7×10^{-3}m ~25×10^{-3}m
Fin Number Range	150~250		150~250	

Table 7. Design parameters of recuperator for OABC

	Hot Side	**Cold Side**
Inlet/outlet temperature [°C]	458/156	128/432
Inlet pressure [kPa]	106	282
Limited Pressure drop ratio	0.03	0.03
Mass flow rate [kg/s]	29.9	29.9
Exchange Heat	9.47MW	

Table 8. PFHE core design results

	Secondary heat exchanger	**Recuperator**
HX width [m]	2.0	2.0
HX length [m]	0.372	1.86
HX height [m]	0.973	2.66
Hot Fin height [m]	0.0012	0.0043
Cold Fin height [m]	0.0035	0.0053
Hot Fin thickness [m]	0.00010	0.00010
Cold Fin thickness [m]	0.00030	0.00030
Hot Fin gap [m]	0.00010	0.0022
Cold Fin gap [m]	0.00028	0.0028
Hot Fin offset length [m]	0.003	0.008
Cold Fin offset length [m]	0.007	0.007
Number of hot side layers	170	250
Number of cold side layers	171	251
Plate thickness [m]	0.0005	0.0005
Core Volume [m^3]	**0.724**	**9.88**
Hot side pressure drop [kPa]	6.56	14.61

Cold side pressure drop [kPa]	8.04	4.73
Heat exchanger effectiveness [%]	95.1	92.2

2.3 Heat Exchanger Desing for Closed sCO_2 Brayton Cycle

PCHEs consist of many plates chemically etched with a plentiful number of micro-wavy channels on each plate and are diffusion bonding at high pressure and high temperature [11]. This increases the heat transfer area of PCHE, resulting in high heat exchange efficiency and small volume and can endure high pressure of 50MPa and high temperatures of 800°C [12]. Owing to the capability of PCHEs to adequately maintain the operational conditions requisite for CCBCs they have been chosen to facilitate heat exchange processes within CCBC systems. The channel types for PCHE include straight and zigzag. Compared to straight channel and zigzag channel, volume of the zigzag channel type was reduced volume by 16% as referring previous work [13]. Therefore, zigzag channel type was selected in this study for design and analysis.

MSR heat exchanger was selected a counter-flow type and zigzag channels as shown in Figure 6. Rectangular cross section of PCHE is shown as Figure 7. As shown in Figure 7, channel consists of channel width ($= D_h, D_c$), plate thickness ($= t_{min}$) and ridge width ($= t_{rid}$) for the heat exchanger. The PCHE is optimized through changing the channel width, number of channel and the length of the heat exchanger. The plate material is selected as SS316L and plate thickness, ridge width, zigzag angle ($= \alpha$) and wavelength ($= l_{wave}$) were set to 1.0mm, 0.5mm, 32.5° and 9mm, respectively [14].

In the sCO_2 power conversion cycle, the size of the precooler was also considered. Table 9 shows the fixed and changed channel geometry of zigzag channel for secondary heat exchanger, recuperator and precooler. In addition, design parameters of intermediate loop and power conversion are shown in Table 4 above, and the recuperator design parameters of hot and cold side of the recuperator and the recuperator are shown in Table 10 and 11 respectively, which is obtained by cycle optimization.

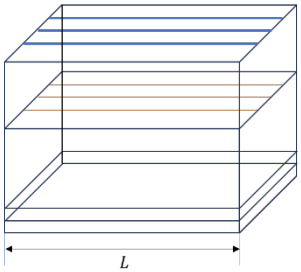

Figure 6. Schematic of counter-flow zigzag channel PCHE

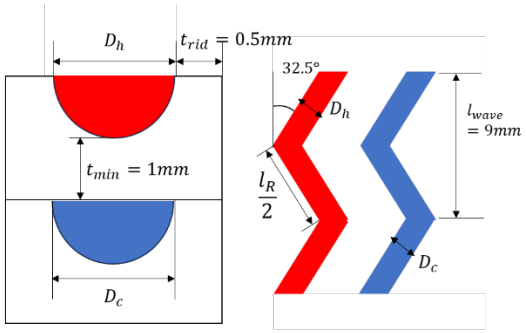

Figure 7. Channel geometry of designed Intermediate heat exchanger

The correlation of the friction factor and Nusselt number for CO_2 with zigzag angle by 32.5° are following Equation 3 and 4, which is suggested by Kim [15]. According to Yoon et al, the correlation of the friction factor and Nusselt number for intermediate loop salt with sharp-edged zigzag channel are following Equation 5 and 6, where l_R is the relative length defines as $l_R = l_{wave} \cos\alpha$, and D_{eq} is hydraulic diameter for the semi-circular channel [16].

$$f = 0.2515 \times Re^{-0.20315} \quad for\ 2000 < Re < 58000 \quad (3)$$

$$Nu = 0.02925 \times Re^{0.8138} \quad for\ 2000 < Re < 58000 \quad (4)$$

$$f = \frac{15}{Re} + \frac{6.728}{1000}\exp(6.6705 * \alpha)\left(\frac{l_R}{D_{eq}}\right)^{-2.3833*\alpha+2+6648\times10^{-1}} + \frac{4.3551*\alpha-1.0814}{100} \quad for\ 50 \le Re \le 2000 \quad (5)$$

$$Nu = (0.71\alpha + 0{,}289)\left(\frac{l_R}{D_{eq}}\right)^{-0.087} Re^{-0.11(\alpha-0.55)^2-0.004\left(\frac{l_R}{D_h}\right)\alpha+0.54} Pr^{0.56} \quad for\ 550 < Re < 2000 \quad (6)$$

Table 9. Design parameters of PCHE

	Secondary Heat Exchanger	Recuperator	Precooler
Hot channel width	1.55×10^{-3}m ~2×10^{-3}m	1×10^{-3}m ~2×10^{-3}m	1.7×10^{-3}m ~2×10^{-3}m
Cold channel width	1.55×10^{-3}m ~3×10^{-3}m	1×10^{-3}m ~3×10^{-3}m	1.7×10^{-3}m ~2×10^{-3}m
Number of hot channels	25100~148000	25100~148000	25100~148000
Number of cold channels	25100~148000	25100~148000	25100~148000
Heat exchanger length	0.1m~1.8m		
Plate thickness	1mm		
Ridge width	0.5mm		
Zigzag angle	32.5°		
Wave length	9mm		

Table 10. Design parameters of recuperator for CCBC

	Hot Side	Cold Side
Inlet/outlet temperature [°C]	499/183	156/427
Inlet pressure [kPa]	8.74	25000
Limited Pressure drop [kPa]	250	100
Mass flow rate [kg/s]	25.5	25.5
Exchange Heat	9.27 MW	

The optimization process was carried out using in house code called KAIST_PCHE_v1.2. Since PCHE has a repeated channel configuration, the total thermal hydraulic performance in PCHE can be estimated by dividing the section [14]. This code calculates the heat exchange performance and pressure drop of the heat exchanger to obtain the next mesh condition. The algorithm of this code is shown in Figure 8. Finally, the temperature and pressure on the opposite side are obtained, and iteration is performed until the error with the input data on the cold side becomes 10^{-4}. Given the range of the geometry, the optimized design parameters with the minimum volume are obtained.

The design results of secondary heat exchanger, recuperator and precooler are shown in Table 12. The smallest volume of secondary heat exchanger, precooler and recuperator is 0.0768m^3, 0.0335m^3 and 0.283m^3 respectively.

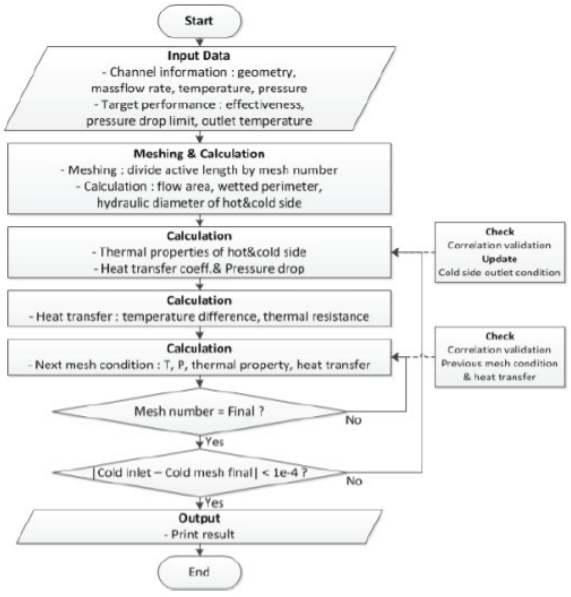

Figure 8. Algorithm of the KAIST_PCHE_v1.2

Table 11. Design parameters of precooler for CCBC

	Hot side (CO_2)	Cold Side (water)
Inlet/outlet temperature [°C]	183/60	35/25
Inlet pressure [kPa]	8495	300
Limited Pressure drop [kPa]	100	100
Mass flow rate [kg/s]	25.5	101
Exchange Heat	4.24 MW	

Table 12. PCHE core design results

	Secondary Heat Exchanger	Precooler	Recuperator
HX width [m]	0.723	0.50086	0.63388
HX length [m]	0.147	0.13385	0.70521
HX height [m]	0.723	0.50086	0.63388
Hot channel width [m]	0.00155	1.7	0.002
Cold channel width [m]	0.00155	1.7	0.003
Hot channel ridge [m]	0.0005	0.0005	0.0005
Cold channel ridge [m]	0.0005	0.0005	0.0005
Number of hot channels	55825	25100	25100
Number of cold channels	55825	37000	25100
Plate thickness [m]	0.001	0.001	0.001
Core Volume [m^3]	**0.0768**	**0.0335**	**0.283**
Hot side pressure drop [kPa]	8.39	45.8	227
Cold side pressure drop [kPa]	22.34	43.12	9.94
Hot side average Re	129	44234	28389
Cold side average Re	11901	4529	16185
Heat Load [MW]	6.44	4.28	9.29

3. Summary & Further work

The comparison of air and sCO_2 power conversion cycles for 6.5 MWth output was performed. The results of cycle optimization and thermal sizing were used for the comparison. Both cycles were successfully optimized. Using the optimized value, the minimum volume of PFHE, which was selected as the heat exchanger for the Open Air Brayton Cycle, was identified. For the Closed sCO_2 Brayton Cycle, the minimum volume of PCHE, which was selected as the heat exchanger type for the cycle, was obtained by utilizing the results of previous study. The optimized cycle properties are shown in the Table 13.

Table 13. Result of the optimized each cycle

	OABC	CCBC
Cycle Net Efficiency [%]	34.6	34.7
Volume of total heat exchanger [m^3]	10.60	0.393
Cycle specific Work [kW/kg]	75.3	88.4

It was confirmed that the recuperator occupies the largest volume among the components. Given that the fluids on the hot side and cold side are of the same type, it is reasoned that a substantial volume and surface area for heat exchange are necessary. Consequently, the recuperator of the Open Air Brayton Cycle exhibits a volume of 9.8823m^3, significantly larger than the 0.28335m^3 volume of the Closed sCO_2 Brayton Cycle's recuperator. This substantial difference in volume between the two cycles highlights the significantly smaller volume of the Closed sCO_2 Brayton Cycle in comparison to the Open Air Brayton Cycle.

To ensure accurate economic evaluation, it is essential to consider installation costs. We aim to address this aspect in subsequent research endeavors. Moreover, the

size volume of the CCBC shows sufficient enough to flexible applications. Therefore, in next research, we will evaluate to feasibility and economic of the CCBC.

ACKNOWLEDGEMENT

This work was supported by the National Research Foundation of Korea(NRF) grant funded by the Korea government(MSIT) (RS-2023-00259713).

REFERENCES

[1] Serp, Jérôme, et al. "The molten salt reactor (MSR) in generation IV: overview and perspectives." Progress in Nuclear Energy 77 (2014): 308-319.
[2] Olumayegun, Olumide, Meihong Wang, and Greg Kelsall. "Closed-cycle gas turbine for power generation: A state-of-the-art review." Fuel 180 (2016): 694-717.
[3] Kwon JS, Son S, Heo JY, Lee JI. Compact heat exchangers for supercritical CO2 power cycle application. Energ Conver Manage. 2020;209:112666.
[4] Son, In Woo, et al. "Thermal-sizing of the molten salt reactor system with gas Brayton cycle." System 12 (2021): 14
[5] Zohuri, Bahman, Pat McDaniel, and Cassiano de Oliveira. "High Temperature Recuperated Open Air Brayton Cycle for the Next Open Air Brayton Cycle for the Next Generation Nuclear Plant.".
[6] Le Moullec, Yann, et al. "Shouhang-EDF 10MWe supercritical CO2 cycle+ CSP demonstration project." 3rd European Conference on Supercritical CO2 (sCO2) Power Systems. Vol. 2019. No. 19th-20th. 2019.
[7] Gierszowski, P., B. Mikic, and N. Todreas. "Property correlations for lithium, sodium, helium, flibe and water in fusion reactor applications." (1980).
[8] Son, In Woo, et al. "Design study of heat transport and power conversion systems for micro molten salt reactor." International Journal of Energy Research 46.11 (2022): 15441-15462.
[9] Raja BD, Jhala RL, Patel V. Multiobjective thermo-economic and thermodynamics optimization of a plate–fin heat exchanger. Heat Transf Asian Res. 2018;47(2):253-270.
[10] Manglik RM, Bergles AE. Heat transfer and pressure drop correlations for the rectangular offset strip fin compact heat exchanger. Exp Therm Fluid Sci. 1995;10(2):171-180.
[11] Chai, Lei, and Savvas A. Tassou. "A review of printed circuit heat exchangers for helium and supercritical CO2 Brayton cycles." Thermal Science and Engineering Progress 18 (2020): 100543.
[12] Johnston, Tony, William Levy, and Svend Rumbold. Application of printed circuit heat exchanger technology within heterogeneous catalytic reactors. American Institute of Chemical Engineers, 2001.
[13] Dostal, Vaclav, Michael J. Driscoll, and Pavel Hejzlar. A supercritical carbon dioxide cycle for next generation nuclear reactors. Diss. Massachusetts Institute of Technology, Department of Nuclear Engineering, 2004
[14] Baik, Seung Joon, et al. "Printed circuit heat exchanger design, analysis and experiment." NURETH-16 (2015). ANS, 2015.
[15] Kim, Seong Gu, et al. "CFD aided approach to design printed circuit heat exchangers for supercritical CO2 Brayton cycle application." Annals of Nuclear Energy 92 (2016): 175-185.
[16] Yoon, Su-Jong, et al. "Development and validation of Nusselt number and friction factor correlations for laminar flow in semi-circular zigzag channel of printed circuit heat exchanger." Applied Thermal Engineering 123 (2017): 1327-1344.